Resonant Raman scattering of nanocavity-confined acoustic phonons

N. D. Lanzillotti-Kimura,[1,2,*] A. Fainstein,[1] B. Jusserand,[2] and A. Lemaître[3]
[1]*Centro Atómico Bariloche and Instituto Balseiro, CNEA, R8402AGP S. C. de Bariloche, R. N., Argentina*
[2]*Institut des Nanosciences de Paris, UMR 7588, CNRS–Université Paris 6, 75015 Paris, France*
[3]*Laboratoire de Photonique et de Nanostructures, CNRS, Route de Nozay, 91460 Marcoussis, France*
(Received 12 July 2008; revised manuscript received 5 December 2008; published 7 January 2009)

A structure that is a resonator for photons and acoustic phonons and can be furthermore tuned to an exciton resonance is investigated. We present Raman-scattering experiments under double optical resonance, and we study the possibility of further enhancing the photon-phonon interaction by resonantly exciting an electronic state confined in the acoustic nanocavity spacer. We show that through this electronic resonance the confined acoustic mode can be amplified. In addition, we report the presence of features corresponding to the Brillouin zone edge and oscillations related to finite-size effects. A comparison with photoelastic model simulations is presented, showing a good agreement with the observed spectral features.

DOI: 10.1103/PhysRevB.79.035404 PACS number(s): 78.67.Pt, 63.22.Np, 78.30.−j, 78.67.De

I. MOTIVATION

Semiconductor optical microcavities are structures that enable the spatial and spectral confinement and amplification of light.[1,2] They work in a similar way to a Fabry-Perot resonator, where two mirrors are separated by a spacer. In the case of semiconductor microcavities, two distributed Bragg reflectors (DBRs) enclose the optical spacer. The amplification and confinement characteristics are determined by the selection of materials, thicknesses, and number of periods of each DBR.[2] They have been used in different experiments, including the modification of photon lifetimes,[3] parametric oscillations,[1] polaritonic Bose-Einstein condensation,[4,5] polariton laser,[6,7] and Raman signal amplification[2] to name a few. Acoustic nanocavities are the elastic equivalent of the photonic devices.[8–11] The optical DBRs are replaced by acoustic Bragg mirrors (BRs). The contrast in the acoustic impedance, i.e., the product of the mass density and the sound velocity, is a relevant parameter to determine the reflecting and confinement characteristics. Nanocavities can confine acoustic phonons in the technologically important terahertz range, concentrating and amplifying the strain in the central spacer. A cavity for light and sound (CLS) is a double resonator that combines an acoustic nanocavity and an optical microcavity in a single monolithic structure.[10–12] In this device, the acoustic resonator is the optical spacer of the microcavity. The electromagnetic field intensity corresponding to the energy of the optical mode presents a maximum in the center of the optical spacer. Under these circumstances, a maximum of the electromagnetic field can be matched with the center of the acoustic cavity, where the strain also presents a maximum, leading to an amplification of the Raman signal.

In Raman experiments in optical microcavities, due to the standing-wave character of the photons within the structure, features normally observed in both backscattering (BS) and forward-scattering (FS) geometries become simultaneously observable. Acoustic confined modes have been detected and studied in Raman-scattering experiments performed in CLS.[10,11] The confinement effects of light pulses in coherent phonon generation experiments performed on CLS have also been recently studied, showing similar selection rules and enhancement behavior as observed in Raman experiments.[12]

Besides the described optical confinement, the standard way to enhance a Raman signal is through electronic resonances. Such resonant Raman scattering by acoustic phonons was previously studied in great detail in semiconductor superlattices.[13–18] A continuous emission background and peaks and dips related to the folded phonon-dispersion gaps were observed. In these cases, the distribution of electronic confinement energies due to random variations in layer thicknesses allows Raman processes strongly resonant with individual quantum wells, causing a partial breakdown of the crystal momentum selection rules. In such situations, q_z is not a good quantum number and is not conserved. Finite-size effects also introduce a relaxation of the selection rules, and Raman scattering from forbidden modes can become observable.[19–21] Resonant Raman scattering by confined phonons in acoustic cavities was introduced in Ref. 22.

The acoustic, optical, and electronic characteristics of the CLS can be engineered to obtain a fully optimized structure where the acoustic and optical cavity mode energies are conveniently set and the electronic transitions are fixed at desired values. In this work, we study the possibility of further enhancing the photon-phonon interaction in a CLS by resonantly exciting an electronic state confined in the acoustic nanocavity spacer. This gives rise to the enhancement of several spectral features, particularly, of the acoustic cavity mode. We investigate the effects of the artificially introduced acoustic modulation when the acoustic spacer is resonantly excited. A simple theoretical model based on photoelastic interactions is introduced to explain the observed features. This paper is organized as follows. Section II briefly describes the sample design; double optical resonance (DOR) experiments are described in Sec. III. In Sec. IV we present the results on resonant Raman scattering from CLS. Finally, conclusions are presented in Sec. V.

II. CAVITIES FOR LIGHT AND SOUND

The studied sample consists of an acoustic nanocavity embedded in an optical microcavity. The sample was grown

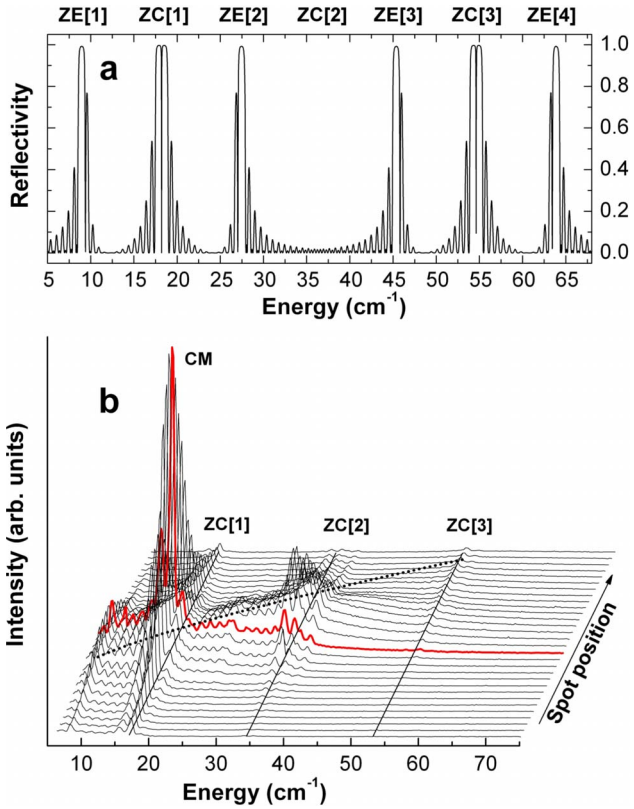

FIG. 1. (Color online) Top panel: calculated reflectivity of the acoustic nanocavity. Bottom panel: measured Raman-scattering spectra varying the spot position on the sample taken at room temperature with an incidence angle of ~15° and a laser wavelength of 815 nm (see text for details). Continuous lines indicate the acoustic band-gap positions; the dotted line is a guide to the eyes for the optical mode spectral position. CM, ZC[2], and ZC[3] stand for cavity mode in the first minigap at the Brillouin zone center, and second and third folded acoustic phonons at the Brillouin zone center, respectively.

on a (001) GaAs substrate by molecular-beam epitaxy. The acoustic nanocavity is formed by two 12 period of 82/23 Å AlAs/GaAs (Ref. 23) superlattices (SLs) enclosing a $\lambda_s/2$ (46 Å) GaAs spacer, where λ_s is the acoustic wavelength of the confined cavity mode. The chosen thickness relation ($\sim 3\lambda_s/4$, $\sim\lambda_s/4$) maximizes the first minigap at the Brillouin zone center. The nominal energy of the confined acoustic mode is ~18 cm^{-1}. The upper panel of Fig. 1 shows the reflectivity of the acoustic nanocavity. Six high-reflectivity bands can be observed corresponding to acoustic minigaps in the dispersion relation. ZE[n] (ZC[n]) stands for nth folded acoustic modes at the Brillouin zone edge (center). In ZC[1] and ZC[3] there is a confined mode centered in the high-reflectivity bands; while in the rest of the minigaps the confined modes are not centered. The second minigap at Brillouin zone center (ZC[2] at ~35 cm^{-1}) is closed; thus there is no associated high-reflectivity band, and no confined mode appears.

The acoustic nanocavity constitutes, as a whole, a λ_l optical spacer, where λ_l is the optical wavelength of the confined microcavity mode. The optical DBRs are formed by 628/728 Å $Al_{0.2}Ga_{0.8}As$/AlAs (Ref. 23) bilayers. The top (bottom) DBR is 10 (14) periods thick. An asymmetric number of DBR pairs is chosen in order to compensate the difference of the air/sample and sample/substrate reflectivities. The sample presents a gradient in the thickness in order to allow the tuning of both the incident laser and the scattered light with the optical cavity mode by changing the spot position. The optical resonance can be furthermore tuned by varying the laser energy and the incidence angle.[24,25]

Due to confinement effects, the electronic transitions in the GaAs layers that form the acoustic BRs are higher in energy than that corresponding to the acoustic spacer. The electronic transition of the acoustic spacer is at 732 nm, determined by photoluminescence (PL) experiments performed at 80 K. This value was confirmed using envelope function model calculations. We estimate the transition of the GaAs layers in the BRs to be at ~650 nm using the same model.

By changing the position of the spot on the sample, it is possible to change the relative energy difference between the cavity mode and the electronic transition of the acoustic spacer. The optical cavity mode is more sensitive to the spot position than the electronic levels (determined mainly by the bulk energy gap) and the acoustic cavity mode energy (the involved energies are much smaller and the variation in the 30 cm^{-1} phonon across the sample is less than 1.5 cm^{-1}).

III. DOUBLE OPTICAL RESONANCE

We measured Raman-scattering spectra in backscattering geometry using a tunable Ti-sapphire laser. The collected spectra were dispersed using a triple T64000 Jobin-Yvon Raman spectrometer equipped with a liquid-N_2 cooled charge-coupled device (CCD). To perform the Raman-scattering experiments from the CLS, we collected the scattered light in the normal direction. Since the sample was grown with a gradient in the thickness, the energy of the optical mode changes with the spot position. When the energy of the scattered photons coincides with the energy of the optical cavity mode, we are in the standard (outgoing) simple optical resonance. In the lower panel of Fig. 1 we show the measured Raman-scattering spectra at room temperature (RT) for different spot positions for a fixed incidence angle of ≈15° and a laser energy of 1.521 eV (815 nm). The electronic transition of the acoustic spacer is estimated to be at 1.594 eV (778 nm) at RT, which was determined by the PL measurements at 80 K and gap evolution with temperature. Features in the Raman spectra between 8 and 50 cm^{-1} are clearly observable in a single measurement due to the relatively low finesse of the optical cavity (~300). Continuous lines at ~17.3, 34.5, and 53.0 cm^{-1} indicate the positions of the folded acoustic phonons at the Brillouin zone center (ZC[1], ZC[2], and ZC[3], respectively). The dotted line is a guide to the eyes for the spectral position of the optical mode, which changes between 10 and 60 cm^{-1}. Note that the selective amplification of the emission of phonons is accomplished when the optical mode passes through them, in particular, the peaks at ~17.3 (corresponding to ZC[1]) and 34.5 cm^{-1} (ZC[2]) present a maximum. Note also the presence of oscillations between minigaps.

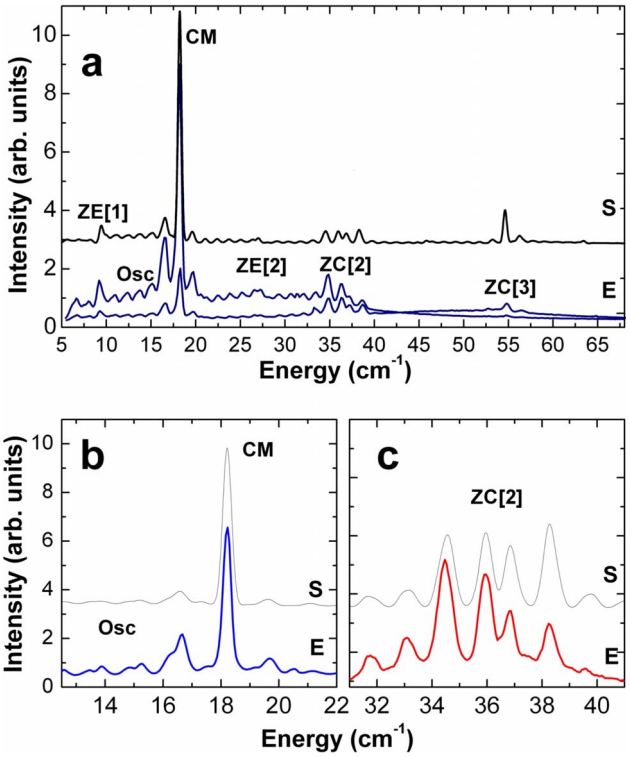

FIG. 2. (Color online) Panel (a): experimental (E) and simulated (S) Raman spectra. The experimental curves correspond to two different double optical resonance conditions (different incidence angles) taken at room temperature and an excitation laser of 815 nm. The simulated spectrum was Gaussian convoluted to account for the experimental resolution (0.40 cm^{-1}) and arbitrarily scaled to match the experimental intensity. Panels (b) and (c) show detail of the first and second zone-center band-gap regions measured with a resolution of 0.15 cm^{-1} (see text for details).

We can take advantage of the in-plane photon mode dispersion of the optical microcavity to enhance the scattering. By changing the spot position on the sample, it is possible to achieve the scattered photon resonance; while changing the incidence angle it is possible to tune the incoming photon resonance. This condition is called DOR.[11,24,25] The thick curve in Fig. 1(b) corresponds to the DOR condition which maximizes the peak at 17.3 cm^{-1}, corresponding to the confined acoustic cavity phonons in the first minigap at the Brillouin-zone-center CM [incidence angle of ~15° and laser energy at 1.521 eV (815 nm)]. Observe how the CM peak is amplified when the DOR condition is achieved, presenting a maximum.

The maximum at 34.5 cm^{-1} in Fig. 1(b) does not represent a DOR condition; it is the result of a balance between the single optical resonance (outgoing photons) and the optical cavity mode at 15° that is detuned from the laser energy. In other words, moving the spot on the sample improves the single outgoing optical resonance for this energy, while the incoming photons are more detuned from the optical cavity mode. However, the incidence angle and spot position can be chosen in such a way that the DOR condition is achieved to maximize different spectral features, in particular, the ZC[2] modes.[24,25]

In panel (a) of Fig. 2 we present experimental and simulated Raman spectra taken at RT and a laser energy of 1.521 eV (815 nm). The experimental curves correspond to two different DOR conditions, maximizing the signal at ZC[1] and ZC[3], respectively. The simulations were performed using a photoelastic model, considering a nominal structure and assuming that both incident and scattered electromagnetic fields have the same (resonant) spatial distribution. The simulated spectrum was Gaussian convoluted to account for the experimental resolution (0.4 cm^{-1}). Observe that features related to ZE[1], ZC[1], ZE[2], ZC[2], and ZC[3] can be clearly observed. Panels (b) and (c) in Fig. 2 present a detailed high-resolution (0.15 cm^{-1}) spectrum of the ZC[1] [Fig. 2(b)] and ZC[2] [Fig. 2(c)] energy regions. In the spectrum shown in Fig. 2(b) we can identify an intense acoustic CM and side oscillations (Osc.) related to finite-size effects. Peaks between Osc and CM arise from contributions from the whole acoustic cavity structure and are a mixture of modes normally observable in backscattering and forward-scattering geometries with no optical confinement. It must be noted that these modes do not have a defined symmetry. The spectrum shown in Fig. 2(c) presents four principal peaks and side oscillations. Of these four principal peaks, the two external peaks are normally observable in BS geometry without optical confinement, while the two central peaks correspond to the peak normally observable in FS geometry, split by the interference between the two acoustic mirrors.[20] As previously stated, at ZC[2] there is no confined mode. The strain associated to the observed acoustic modes in this energy band is odd in the acoustic spacer layer, so all the contributions to the Raman signal come from the SLs. In this way, CM is mainly sensitive to the electron-phonon interaction within the acoustic spacer, while modes at ZC[2] are only sensitive to interactions within the BRs.

The observation of ZE peaks and side oscillations in Fig. 2(a) is attributed to an excitonic resonance. In what follows we will address the analysis of the amplification of the CM and other features due to this excitonic resonance, while maintaining the DOR condition.

IV. EXCITONIC RESONANT RAMAN SCATTERING

To study the excitonic resonance effects we performed Raman-scattering experiments, changing the excitation laser wavelength between 765 and 800 nm, conserving always the DOR condition, and below any absorption in the acoustic nanocavity. The 765 nm limit of the optical cavity mode is set by the sample edge. In order to have a low enough photoluminescence background (coming from the acoustic spacer) as compared to the resonant Raman signal, all the experiments were performed at 80 K. In the first series of experiments, the DOR condition is tuned to maximize CM [as in Fig. 2(b)]. Panel (b) of Fig. 3 shows the measured Raman spectra (narrow features on top of a luminescence background coming from the GaAs substrate filtered by the optical cavity mode) as a function of the incident laser wavelength. This photoluminescence background is indicated for a single spectrum in gray. Each spectrum is taken at a different spot on the sample in order to tune the cavity mode

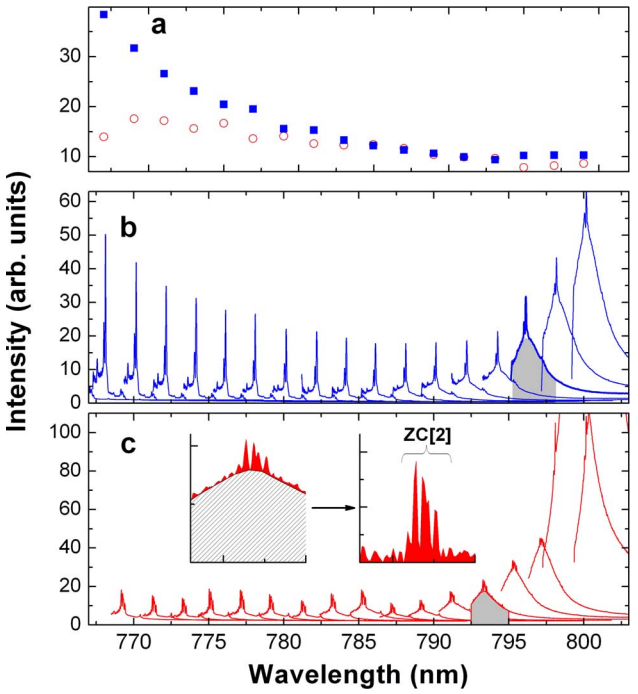

FIG. 3. (Color online) Panel (a): cavity mode (black squares) and second zone-center peak (circles) intensity as a function of excitation laser wavelength derived from the spectra in panels (b) and (c). Panels (b) and (c): Raman-scattering spectra as a function of the excitation laser under double optical resonant condition for the CM and ZC[2] features, respectively (taken at 80 K). Gray zones indicate the photoluminescence background. Insets show a spectrum with and without the photoluminescence background subtracted.

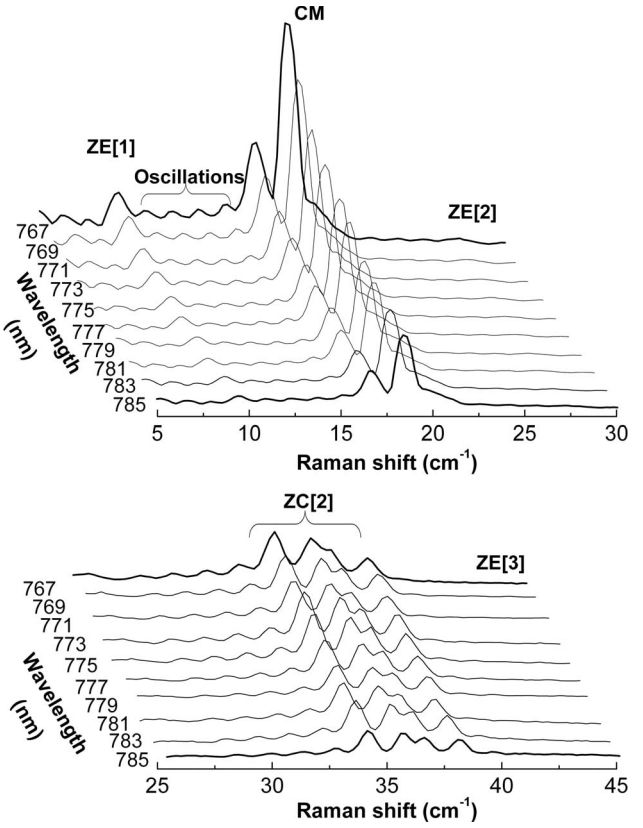

FIG. 4. Measured Raman spectra as a function of the laser wavelength for the CM (top panel) and the ZC[2] modes (bottom panel) taken at 80 K. ZE, CM, and ZC stand for zone edge, cavity mode, and zone-center modes, respectively.

with the Raman-scattered photons. Note that as the laser approaches the acoustic spacer electronic transition (~735 nm), the Raman spectra increase in intensity. The second series of experiments was performed by localizing the DOR on ZC[2] [panel (c) of Fig. 3]. Contrary to the CM behavior, ZC[2] features present an almost constant intensity. This agrees with the fact that these modes are independent of the resonant condition in the spacer. The insets of Fig. 3(c) present a single Raman spectrum as measured (left), with the substrate photoluminescence background indicated in gray, and the Raman spectrum after the background subtraction (right). Panel (a) of Fig. 3 plots the intensities of the CM (squares) and the ZC[2] modes at ~35 cm^{-1} (empty circles) as a function of the laser wavelength. It is clear that the CM is selectively amplified with respect to the ZC[2] modes. The slowly varying intensity of the ZC[2] features can be attributed to the weak resonant behavior of the electronic transition of the SLs layers (at ~650 nm).

Figure 4 shows the detailed measured Raman spectra for different laser wavelengths (indicated on the left), for the DOR condition centered at the CM (top panel) and ZC[2] (bottom panel). In the top panel it can be observed how the cavity mode is amplified as the laser approaches the excitonic resonance. In addition to this amplification of the CM, two additional features must be pointed out. On one hand, on the left side of the cavity mode (lower Raman shift), finite-size-like oscillations are also resonantly amplified (Osc in Fig. 2); on the other hand, Brillouin-zone-edge features located at 9.3 and 26.8 cm^{-1} (ZE[1] and ZE[2]) appear as the laser approaches the electronic energy level of the acoustic cavity spacer. As we will show next, the amplification of the CM peak with respect to ZC[2], along with the observation of the rest of the features, is a clear manifestation of the modulation of the elastic properties in the structure, combined with a resonant excitation selectively localized at the cavity spacer. The ZC[2] spectra shown in the bottom panel are characterized by the presence of four peaks with an intensity that is independent of wavelength. Weak side oscillations can also be noticed on the lower-energy side of the spectra.

In order to describe the behavior of the spectra as the resonant condition is approached, we performed simulations based on a photoelastic model. The expression for the Raman efficiency is given by[11,12,26–28]

$$\sigma(\omega) \propto \frac{1}{\omega}[n(\omega)+1]\left|\int dz E_L(z)E_S^*(z)p(z)\frac{\partial u(z)}{\partial z}\right|^2, \quad (1)$$

where $n(\omega)$ is the Bose-Einstein statistical factor, $p(z)$ is the material-dependent photoelastic constant (assumed constant in each layer), $u(z)$ is the atomic displacement within the structure, and E_L and E_S are the incident and scattered electric fields, respectively. The electric fields are calculated using a standard matrix method implementation with appropri-

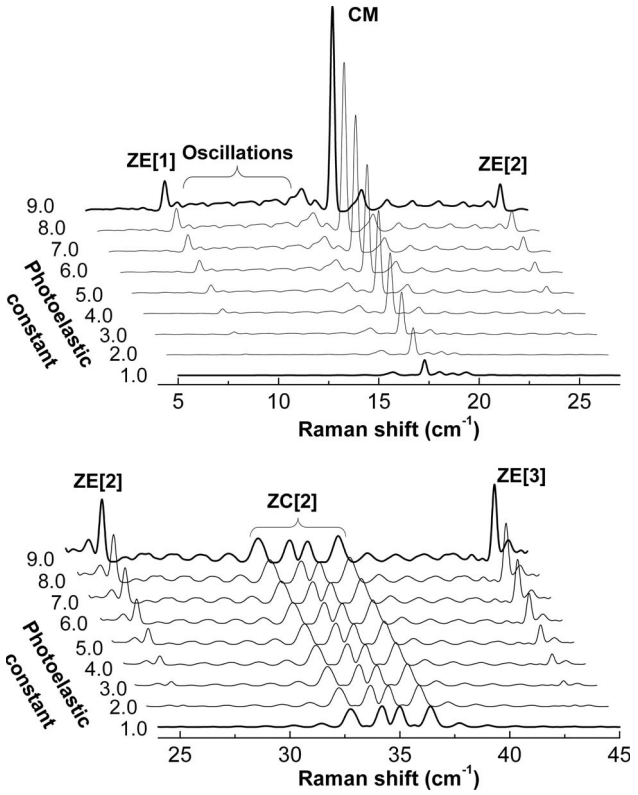

FIG. 5. Simulated Raman spectra as a function of the photoelastic constant of the acoustic cavity spacer. On the left, the numbers indicate the factor by which the nominal photoelastic value is multiplied. ZE, CM, and ZC[2] stand for zone edge, cavity mode, and second folded phonons at zone center, respectively.

ate boundary conditions. To simplify the calculation, we consider that the incoming and scattered fields have the same spatial distribution. The phonon displacements are obtained using a matrix method implementation of a continuum theory that includes zero-strain boundary conditions at the sample-air interface. We simulate the resonant experiment by changing the photoelastic constant value of the layer that is being resonantly excited. In our case, we use a constant value for all the GaAs layers except for the acoustic cavity spacer which is multiplied by a factor n.

Figure 5 presents the simulated Raman spectra as a function of the photoelastic constant of the acoustic cavity spacer. On the left, the value of the factor n is indicated. In the top (bottom) panel we plot the behavior of CM (ZC[2]) under DOR. From the simulations the following results must be noted. (1) The intensity of the confined cavity mode peak increases as the factor n is increased; its relative height to close features also grows. (2) The general spectral shape changes; on one hand peaks at 7.0 and 26.0 cm^{-1} (ZE[1] and ZE[2]) become observable; on the other hand, strong oscillations between minigaps appear. (3) The intensity of the ZC[2] features is almost constant as the factor n is changed. This is clear when comparing the behavior of the ZE[2] and ZE[3] with ZC[2] peaks in the lower panel of Fig. 5. As commented before, this latter feature can be understood through these simulations due to the fact that the $\partial u(z)/\partial z$ is odd for ZC[2] in the central acoustic cavity layer. On the contrary, the CM has an even $\partial u(z)/\partial z$ distribution through the structure, which furthermore is strongly localized at the resonantly excited acoustic cavity layer.

The resonant excitation, or equivalently, the increase in the photoelastic contribution of the *localized* acoustic spacer produces a mode selective excitation. This spatially localized excitation allowed the observation of peaks at ZE[n], which are not observable under nonresonant excitation. In addition, the oscillations related to finite-size effects[19] are also amplified; their number and relative intensity are given by the number of periods and materials in the acoustic mirrors, respectively. In the simulation shown in Fig. 2 a factor of $n=4.0$ was used in the photoelastic constant corresponding to the acoustic cavity spacer. The agreement between experiments and simulations is remarkable, and the main features of the spectra are reproduced: side oscillations, zone-edge features, cavity mode, side modes, and ZC[2] features. However, oscillations on the high-energy side of the CM observable in the simulations have not been observed in the experiments at low temperatures (see Fig. 4); at RT (Fig. 2) oscillations at both sides of the CM are present and equally intense, which is in agreement with the model calculations.

V. CONCLUSIONS

The presented results demonstrate that it is possible to perform a selective excitation of acoustic confined cavity phonons in Raman-scattering experiments by tuning the laser with an exciton confined in the cavity spacer. The use of an optical cavity allows the detection of light scattered by phonons with $q=0$ and amplifies the electromagnetic field enhancing the Raman cross section of the system. A proper selection of thicknesses determines the electronic transitions in the layers that form the acoustic cavity in such a way that is possible to excite only one of them, in particular, the cavity spacer.

As previously demonstrated for SLs, the resonant excitation of a single layer gives rise to strong modifications of the measured spectra. The modification of the phonon density of states activates additional peaks generated by phonons in minigaps at the Brillouin zone edge. These modes are not normally observable under a nonresonant condition. The described engineering of acoustic phonons, and of the photonic and electronic states, provides interesting alternatives for the study and the generation and control of coherent terahertz hypersound with light.

ACKNOWLEDGMENTS

This work was supported by a SECyT-ECOS(Sud) collaboration. N.D.L.K. acknowledges support from Fundación YPF (Argentina) and Programme Alβan under Scholarship No. E06D103192AR. A.F. also acknowledges support from ANPCyT through Grant No. PICT2004 25316. The authors acknowledge R. Teissier for the code of energy-level calculations in heterostructures. N.D.L.K. thanks J. Groenen for fruitful and enlightening discussions.

*kimura@cab.cnea.gov.ar

[1] M. S. Skolnick, T. A. Fisher, and D. M. Whittaker, Semicond. Sci. Technol. **13**, 645 (1998).
[2] A. Fainstein and B. Jusserand, in *Light Scattering in Solids IX*, edited by M. Cardona and R. Merlin (Springer, Heidelberg, 2007).
[3] B. Sermage, S. Long, I. Abram, J. Y. Marzin, J. Bloch, R. Planel, and V. Thierry-Mieg, Phys. Rev. B **53**, 16516 (1996).
[4] J. Kasprzak, M. Richard, S. Kundermann, A. Baas, P. Jeambrun, J. M. J. Keeling, F. M. Marchetti, M. H. Szymanska, R. Andre, J. L. Staehli, V. Savona, P. B. Littlewood, B. Deveaud, and Le Si Dang, Nature (London) **443**, 409 (2006).
[5] Hui Deng, D. Press, S. Götzinger, G. S. Solomon, R. Hey, K. H. Ploog, and Y. Yamamoto, Phys. Rev. Lett. **97**, 146402 (2006).
[6] G. Malpuech, A. Di Carlo, A. Kavokin, J. J. Baumberg, M. Zamfirescu, and P. Lugli, Appl. Phys. Lett. **81**, 412 (2002).
[7] G. Malpuech, A. Kavokin, A. Di Carlo, and J. J. Baumberg, Phys. Rev. B **65**, 153310 (2002).
[8] S. I. Tamura, H. Watanabe, and T. Kawasaki, Phys. Rev. B **72**, 165306 (2005).
[9] N. D. Lanzillotti Kimura, A. Fainstein, and B. Jusserand, Phys. Rev. B **71**, 041305(R) (2005); N. D. Lanzillotti-Kimura, A. Fainstein, C. A. Balseiro, and B. Jusserand, *ibid.* **75**, 024301 (2007).
[10] P. Lacharmoise, A. Fainstein, B. Jusserand, and V. Thierry-Mieg, Appl. Phys. Lett. **84**, 3274 (2004).
[11] M. Trigo, A. Bruchhausen, A. Fainstein, B. Jusserand, and V. Thierry-Mieg, Phys. Rev. Lett. **89**, 227402 (2002); see also J. M. Worlock and M. L. Roukes, Nature (London) **421**, 802 (2003).
[12] N. D. Lanzillotti-Kimura, A. Fainstein, A. Huynh, B. Perrin, B. Jusserand, A. Miard, and A. Lemaître, Phys. Rev. Lett. **99**, 217405 (2007).
[13] T. Ruf, J. Spitzer, V. F. Sapega, V. I. Belitsky, M. Cardona, and K. Ploog, Phys. Rev. B **50**, 1792 (1994).
[14] V. I. Belitsky, T. Ruf, J. Spitzer, and M. Cardona, Phys. Rev. B **49**, 8263 (1994).
[15] T. Ruf, V. I. Belitsky, J. Spitzer, V. F. Sapega, M. Cardona, and K. Ploog, Phys. Rev. Lett. **71**, 3035 (1993).
[16] V. F. Sapega, V. I. Belitsky, T. Ruf, H. D. Fuchs, M. Cardona, and K. Ploog, Phys. Rev. B **46**, 16005 (1992).
[17] M. Cazayous, J. Groenen, A. Zwick, A. Mlayah, R. Carles, J. L. Bischoff, and D. Dentel, Phys. Rev. B **66**, 195320 (2002).
[18] M. Cazayous, J. R. Huntzinger, J. Groenen, A. Mlayah, S. Christiansen, H. P. Strunk, O. G. Schmidt, and K. Eberl, Phys. Rev. B **62**, 7243 (2000).
[19] M. Trigo, A. Fainstein, B. Jusserand, and V. Thierry-Mieg, Phys. Rev. B **66**, 125311 (2002).
[20] M. Giehler, T. Ruf, M. Cardona, and K. Ploog, Phys. Rev. B **55**, 7124 (1997).
[21] P. X. Zhang, D. J. Lockwood, and J.-M. Baribeau, Can. J. Phys. **70**, 843 (1992).
[22] M. F. Pascual Winter, G. Rozas, A. Fainstein, B. Jusserand, B. Perrin, A. Huynh, P. O. Vaccaro, and S. Saravanan, Phys. Rev. Lett. **98**, 265501 (2007).
[23] Material parameters used in the simulations. Sound velocities: 4726, 5630, and 4906.8 m/s; mass densities=5.315, 3.735, and 5.001 g/cm^3; indices of refraction=3.5419, 2.96, and 3.43 for the GaAs, AlAs, and AlGaAs, respectively.
[24] A. Fainstein, B. Jusserand, and V. Thierry-Mieg, Phys. Rev. B **53**, R13287 (1996).
[25] A. Fainstein and B. Jusserand, Phys. Rev. B **57**, 2402 (1998).
[26] B. Jusserand and M. Cardona, in *Light Scattering in Solids V*, edited by M. Cardona and G. Güntherodt (Springer, Heidelberg, 1989).
[27] A. Mlayah, J.-R. Huntzinger, and N. Large, Phys. Rev. B **75**, 245303 (2007).
[28] J. Groenen, F. Poinsotte, A. Zwick, C. M. Sotomayor Torres, M. Prunnila, and J. Ahopelto, Phys. Rev. B **77**, 045420 (2008).